A Control-Free Series Resonant Converter for Battery Charging with Automatic CC-to-CV Profile and Whole-Process High Efficiency

Zhijian Fang, *Member, IEEE*, Haojiang Yue, *Student Member, IEEE*, Zihao Wei, *Student Member, IEEE*, Zihan Zhang, *Student Member, IEEE*, and Zhicong Huang, *Member, IEEE*

***Abstract*—Constant current (CC) and constant voltage (CV) outputs are required by electric vehicle chargers to comply with the battery profile, which are challenges to the wide operating range, accurate current and voltage control, and high efficiency of the battery chargers. This paper proposes a control-free battery charger based on a series resonant converter (SRC) that features an inherent automatic CC-to-CV profile and whole-process high efficiency. Both the CC and CV modes enjoy identical switching sequences and operating waveforms, and the transition of CC-to-CV depends on the load condition. Automatic and smooth CC-CV transition can also be obtained after the CC charging process, thus avoiding the overvoltage charging risk. Detection of battery state and active control for the charging profile can therefore be eliminated, making the proposed battery charger rugged and reliable. The CC and CV outputs are flexibly configurable by setting the operating frequency and designing the turn ratio of the transformer respectively. Moreover, with an assistive circuit, soft switching can be realized for all switches regardless of the operating conditions to achieve a high efficiency throughout the whole charging process. Finally, a 1 kVA prototype is presented to validate the control-free and automatic CC-to-CV profile. High efficiency up to 98.4% is measured during the whole CC and CV charging periods.**

***Index Terms*—Battery charging, constant current, constant voltage, high efficiency, series resonant converter, soft switching.**

Nomenclature

ω_{r}	Resonant angular frequency
A_{e}	Cross-sectional area of the core
B	Magnetic flux density
B_{m}	Maximum magnetic flux density
C'_{p}	Equal capacitance of series C_p and C_r
C_{ds}	Drain-source capacitance of the switchers
C_{p}	Parasitic capacitor
C_{r}	Resonant capacitor
$D_1 - D_4$	Secondary-side diodes
f_{r}	Resonant frequency
$f_{\mathrm{s,max}}$	Maximum switching frequency
f_{s}	Switching frequency
i_{Di}	Current of diodes D_i
i_{in}	Input current
i_{m}	Magnetic current
$I_{\mathrm{o,max}}$	Maximum charging current
i_{off}	Instantaneous current value at turn-OFF time
I_{o}	Output current
$I_{\mathrm{r,RMS}}$	The RMS value of resonant current
i_{r}	Resonant current
i_{Si}	Current of switches S_i
i_{ssi}	Current of damping-circuit S_{si}
k, α, β	Constants of transformer determined by magnetic material
L_{m}	Magnetic inductance
L_{r}	Resonant inductance
n	Turns ratio
N_2	Transformer secondary turns
p	Action number of each switcher during one switching period.
P_{OFF}	Switching loss
$P_{\mathrm{sw.,cond.}}$	Conduction loss of the switchers
$P_{\mathrm{tr.,cond.}}$	Transformer Conduction Loss
$P_{\mathrm{tr.,core.}}$	Transformer Core Loss
R_{d}	Damping resistor
$R_{\mathrm{L,cri}}$	Critical load resistor
R_{L}	Load resistor
$r_{\mathrm{sw.}}$	Switcher ON-resistor
$r_{\mathrm{tr.}}$	Winding resistor of the transformer
$S_1 - S_4$	Primary-side switches
$S_{\mathrm{s1}},\ S_{\mathrm{s2}}$	Damping-circuit switches
t_{off}	Turning-OFF time
T_{r}	Resonant period
T_{s}	Switching period
v_{ab}	Terminal voltages of the primary-side bridge
$V_{\mathrm{bat,max}}$	Maximum battery voltage
V_{bat}	Battery voltage
v_{cd}	Terminal voltages of the secondary-side bridge
v_{Di}	Voltage of diodes D_i
V_{ds}	Drain-source voltage value at turning-OFF time
V_{i}	Input voltage
v_{r0}	Resonant voltage value at $t = t_0$
v_{r1}	Resonant voltage value at $t = T_r/2$
v_{r2}	Resonant voltage value at $t = T_r$

Manuscript received November 26th, 2022; revised March 9th 2023; accepted Apr. 12th, 2023. This work was supported in part by the National Natural Science Foundation of China (51707138 and 52007067) and in part by the Natural Science Foundation of Guangdong Province (2022A1515011581 and 2023A1515011623).(*Corresponding author: Zhicong Huang.*)

Z. Fang, H. Yue, Z. Wei and Z. Zhang are with School of Automation, China University of Geosciences (Wuhan), Wuhan 430074, China, and also with Hubei Key Laboratory of Advanced Control and Intelligent Automation for Complex Systems, Wuhan 430074, China (e-mail: fangjianhust@gmail.com).

Z. Huang is with the Shien-Ming Wu School of Intelligent Engineering, South China University of Technology, Guangzhou 510006, China (e-mail: zhiconghuang@scut.edu.cn).

v_{r}	Voltage of resonant capacitor
v_{Si}	Drain-to-source voltage of switches S_i
v_{ssi}	Drain-to-source voltage of switches S_{si}
V_{T}	Transformer core volume
Z_{r}	Characteristic impedance

I. Introduction

Nowadays, DC-DC converters for battery charging applications are attracting more and more attentions with the developments of electric vehicles (EVs) [1]–[3]. To comply with the battery charging profile, these converters should be controlled to regulate the required constant current (CC) and constant voltage (CV) outputs. However, the battery voltage rises from near zero to the maximum value during the CC charging period, while the battery current drops from the rated value to near zero during the CV charging period. Wide output voltage and current ranges are required for the DC-DC converters, as well as high efficiency. Meanwhile, accurate CC and CV control are also desired to tackle the overcharging risk.

LLC resonant converter is the most popular DC-DC converter for battery charging due to its outstanding advantages of soft switching, high power density and high efficiency [4], [5]. To adjust the wide output voltage and current ranges of battery charging, a wide switching frequency range is required for the LLC resonant converter which results in large power loss and bulky inductor, capacitor, and transformer. Many design methodologies of LLC resonant converter are presented to adapt to the wide voltage range [6]–[8]. But the switching frequency range is still wide, worsening the efficiency and power density. Burst control [9], [10], PWM [11], phase-shift modulation [12], and energy feedback control [13] are proposed to narrow the switching frequency range under the wide load conditions. Synchronous rectifier control [14], variable topology [15], and variable DC-link voltage control [16], [17] are published to extend the voltage gain range. However, additional devices are required in these methods increasing the converter cost and power loss. Moreover, the transfer functions between the switching frequency and output voltage and current are nonlinear resulting in accurate voltage and current control issues.

To address the accurate control issues, feedback control is used to regulate the switching frequency for the resonant converter [18]. But the simple PI controller fails to comply with the nonlinear power features. In [19], the resonant capacitor voltage is used to compensate for the nonlinear characteristics at the cost of additional voltage sensors. [20] builds an inverse function of the nonlinear converter model to linearize the power transfer features. But the dynamic performance is still poor. In [21], an optimal trajectory tracking method is presented to improve the settling time. However, these control methods are complex and lack robustness. Accurate mathematical models are required rising the realization difficulty in practices.

To simplify the control and optimize the efficiency, a control-free battery charger, which features voltage-independent current and current-independent voltage, is attracting more and more attention and has been widely researched for the wireless power transfer (WPT) applications [22]. In [23], several compensation topologies are proposed to obtain CC or CV outputs with fixed switching frequency. The CC and CV modes can be transferred by hopping the switching frequency. In [24], the variable topology is presented to switch CC and CV mode by using the bidirectional switches. However, the mutual inductance between transmit and reception coils are used to acquire the CC and CV features in the above methods, which cannot be applied for wired battery charging converters with tight coupling transformer. The parallel resonant converter is presented to achieve CC and CV outputs by optimal choosing the switching frequency [25]. But the outputs are still affected by the loads. In [26], a $LCL-T$ resonant converter is proposed to achieve the CC feature with a fixed switching frequency and special design. Despite the output current being independent of the voltage, the output voltage is unlimited in this method. Further charging with CC could damage the battery when the battery's natural voltage limit is reached. To address this issue, a $LCL-T$ resonant converter with clamp diodes is proposed in [27] achieving inherent CC and CV limit features. But large reactive current appears in this converter due to the LCL resonant tank. In [28], a novel dual full-bridge LLC resonant converter is presented with inherent CC and CV characteristics, as well as the excellent features of the LLC resonant converter. However, the added full bridge converter increases the power loss and cost.

To address these issues of battery charging applications, this paper proposes a control-free battery charger based on the series resonant converter (SRC) with inherent and automatic CC-to-CV profile and whole-process high efficiency, which perfectly complies with the battery charging requirements. The output current and voltage are only up to the switching frequency and the input voltage is independent of the load, achieving control-free features. A wide operation range and minimum switching frequency variation can be obtained reducing the power loss and difficulty of control and design. Especially, an automatic transition from CC output to CV threshold can be enabled during the battery charging process avoiding the risk of overcharging. High robustness without battery SOC detection can be achieved. Moreover, a damping circuit is added in the SRC to reduce the oscillation and enable all switches to realize soft switching during the whole operating range. A zero phase angle between the input voltage and current is also obtained. High efficiency and control-free features are achieved for the whole CC and CV charging periods, which nicely satisfy the requirements of battery charging.

Compared to the conventional method, three advantages can be achieved by the proposed method.

1) Both ZCS ON and OFF simultaneously are realized over a wide output range in the proposed method, achieving a tiny switching loss for a wide range. Whereas, in the conventional method, only ZVS-ON is realized suffering from hard-OFF. Moreover, the ZVS feature could lose in light load conditions resulting in large switching loss.
2) Second, a zero phase angle between the input voltage and current is obtained during the whole charging pro-

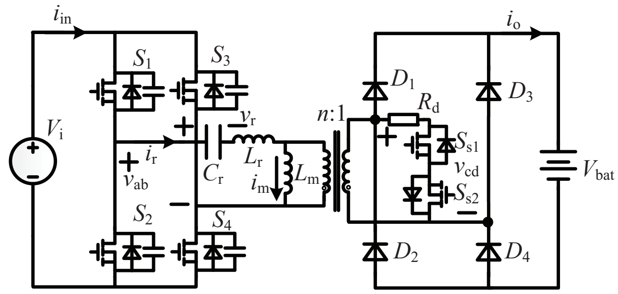

Fig. 1. Schematics of the proposed series resonant converter.

cess in the proposed method. Whereas, large backflow current is needed in the conventional method to regulate the power, which results into large conduction loss.

3) Third, control-free and auto CC-to-CV profile can be achieved in the proposed method to enable high robustness without battery SOC detection. In the conventional method, a current controller and a voltage controller are needed in CC and CV charging period respectively. And a special detection strategy should be used to control the converter transit from CC to CV mode to avoid the overcharge risk.

The rest of this paper is organized as follows. Section II details the proposed modulation scheme in CC and CV mode. The design considerations are presented in Section III. Section IV analyzes the power loss of the proposed converter. Experiments are conducted in Section V to validate the proposed modulation. Finally, Section VI concludes this paper.

II. Proposed Method and Operation Analysis

The proposed topology is shown in Fig. 1, which includes a typical series resonant converter and an assistive damping circuit. The damping circuit includes a bidirectional switch (S_{s1} and S_{s2}) and a damping resistor (R_d) connected across the secondary side of the transformer. The series resonant converter consists of a primary full-bridge circuit and a secondary full-bridge diode rectifier, interconnected with a series resonant tank (L_r–C_r) and a transformer.

The voltage and current waveforms for the series resonant converter are presented in Fig. 2. Note that, the modulation waveforms in CC and CV modes are the same, and thus the transition of CC-to-CV is free of control. S_1 and S_4 are simultaneously turned ON at t_0 and keep ON for $T_r/2$ and T_r respectively, where T_r is resonant cycle. After S_1 is turned OFF, S_2 is ON for $T_r/2$. Then S_1 ˜ S_4 are all turned OFF and the assistive switches S_{s1} and S_{s2} are ON until the end of half switching cycle $T_s/2$. The positive and negative half switching cycles are dualities and thus not repeated.

Consequently, a square voltage v_{ab} waveform with a constant-time high-level state, zero-level state, and variable-time high-impedance state is generated to excite the resonant current. Whereas, the voltage v_{cd} waveform is provided by the secondary rectifier, diodes D_1 – D_4, the states of which are decided by the resonant current i_r. The operation mode of the proposed converter only depends on the load resistance. When

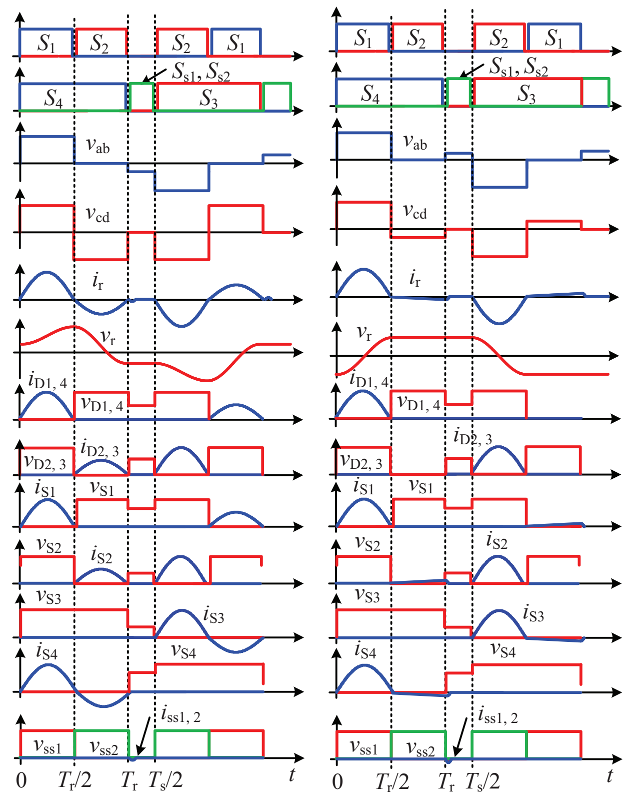

(a) CC mode. (b) CV mode.

Fig. 2. Waveforms of resonant voltage and current with proposed modulation.

the load resistance is small, diodes D_1 ˜ D_4 are turned ON during 0 ˜ T_r, and the converter works in CC mode. Otherwise, the converter is in CV mode. The detailed analysis is given in Sections II-A and -B.

Noticeably again, the switching sequence and operating waveforms are identical for the CC and CV modes. The converter can auto and smooth transfer from CC mode to CV mode with the increase of load resistance.

A. CC Operation Mode

During the CC charging process, the battery voltage $V_{\rm bat}$ is low, providing small equal load resistances. The secondary rectifier is conducted during 0 ˜ T_r, making the converter work in the CC mode. The resonant current and voltage waveforms are illustrated in Fig. 2(a). There are three stages in a half switching cycle in the CC mode. Detailed descriptions are as follows.

1) Stage 1 (t_0 ˜ $T_r/2$): S_1 and S_4 turn ON during this period. That $v_{ab} = V_i$ which is larger than $nV_{\rm bat}$ conducting the rectifier diodes D_1 and D_4. V_i could charge $nV_{\rm bat}$ through resonant tank and transformer, as the circuit shown in Fig. 3 (a). i_r and v_r can be written as

$$i_r = \frac{-v_{\rm r0} + V_i - nV_{\rm bat}}{Z_r}\sin(\omega_r t), \text{ and} \tag{1}$$

$$v_r = (v_{\rm r0} - V_i + nV_{\rm bat})\cos(\omega_r t) + V_i - nV_{\rm bat}. \tag{2}$$

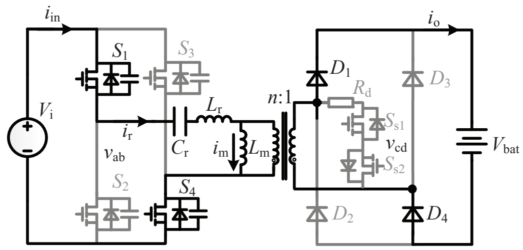

(a) *Equal circuit A.*

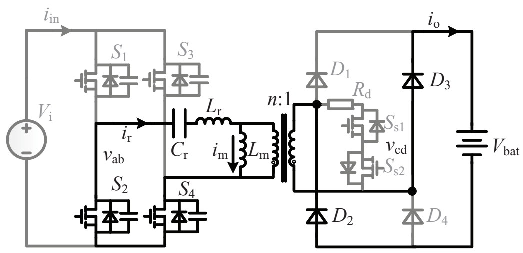

(b) *Equal circuit B.*

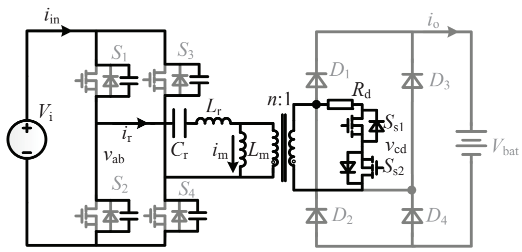

(c) *Equal circuit C.*

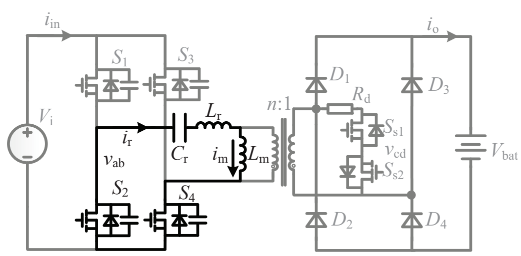

(d) *Equal circuit D.*

Fig. 3. Equivalent circuits of switching stage in the proposed method.

Z_r and ω_r are characteristic impedance and resonant angle frequency respectively defined by

$$Z_r = \sqrt{\frac{L_r}{C_r}},\ \text{and}\ \omega_r = \frac{1}{\sqrt{L_r C_r}}. \tag{3}$$

2) Stage 2 ($T_r/2$ ˜ T_r): After the half resonant cycle, i_r reaches zero again. S_1 turns OFF while S_2 turns ON realizing ZCS ON and OFF. Due to the low battery voltage $V_{\rm bat}$, D_2 and D_3 could conduct during this period, despite $v_{ab} = 0$. The resonant tank continuously charges the battery, as the circuit shown in Fig. 3 (b). i_r and v_r can be expected by

$$i_r = \frac{-v_{\rm r1} + nV_{\rm bat}}{Z_r}\sin[\omega_r(t - T_r/2)],\ \text{and} \tag{4}$$

$$v_r = (v_{\rm r1} - nV_{\rm bat})\cos[\omega_r(t - T_r/2)] + nV_{\rm bat}. \tag{5}$$

3) Stage 3 (T_r ˜ $T_s/2$): After one resonant cycle, all switches turn OFF except S_{s1} and S_{s2}, which shorten the transformer, as the circuit shown in Fig. 3 (c).

At the switching moment, the resonant tank resonates with parasitical capacitance of primate switches S_1 to S_4, and damping resistance $R_{\rm d}$. The equivalent circuit is a RLC series resonant circuit. To suppress the oscillations, the circuit is desired to work in overdamped mode. Then damping resistance is designed as

$$R_d > 2\sqrt{\frac{L_r}{C'_p}}, \tag{6}$$

where $C'_p = \frac{C_p C_r}{C_p + C_r}$.

Due to the small parasitic capacitance and large damping resistances, the oscillation can be quickly supressed and i_r is quickly damped to zero by R_d. i_r is a decay of the transient current without oscillation and v_r could keep $v_{\rm r2}$.

The operation in the negative half switching cycle is similar to the positive one, which is not repeated here. According to the continuity and symmetry of v_r, we have

$$v_{\rm r0} = V_i - 2nV_{\rm bat}, \tag{7}$$

$$v_{\rm r1} = V_i,\ \text{and}, \tag{8}$$

$$v_{\rm r2} = -V_i + 2nV_{\rm bat}. \tag{9}$$

With (1) and (4), the charging current can be calculated as

$$I_o = \frac{2}{T_s}\left(\int_0^{\frac{T_r}{2}} n i_r dt - \int_{\frac{T_r}{2}}^{T_r} n i_r dt\right) = \frac{2nV_i f_s}{\pi Z_r f_r}. \tag{10}$$

The charging current is independent of the output voltage achieving an inherent CC feature. Moreover, we can configure the charging current by choosing the switching frequency.

B. CV Operation Mode

When the battery voltage is charged high enough, the rectifier only conducts during 0 ˜ $T_r/2$ and the converter auto enters into the CV mode. The resonant current and voltage waveforms in this CV mode are illustrated in Fig. 2(b). There are three stages in a half switching cycle in the CV mode.

1) Stage 1 (t_0 ˜$T_r/2$): This stage is the same as Stage 1 in CC mode. V_i charges $V_{\rm bat}$ through the resonant tank. i_r and v_r are identical to (1) and (2), which are not repeated here.

2) Stage 2 ($T_r/2$ ˜T_r): S_2 and S_4 turn ON providing $v_{\rm ab} = 0$. Unlike the CC mode, the rectifier diodes break in this stage due to the high battery voltage, as the circuit shown in Fig. 3 (d). The resonant tank could resonate with the magnetic inductance. Since the magnetic inductance is far larger than the resonant inductance, the small magnetic current could slightly fall which can be regarded as invariable and zero. The resonant voltage could maintain v_{r1} during this period.

3) Stage 3 (T_r ˜$T_s/2$): Similar to Stage 3 in the CC mode, the transformer is shortened thus the magnetic current could fall to zero quickly. The resonant current and voltage keep zero and v_{r1} respectively at this stage.

The operation during the negative cycle is similar. Due to the continuity and symmetry of v_r, we have

$$v_{r0} = -v_{r1}. \tag{11}$$

According to (2), the output voltage is

$$nV_{\rm bat} = V_i. \tag{12}$$

Moreover, the output current can be obtained as

$$I_o = \frac{2}{T_s}\int_0^{\frac{T_r}{2}} n i_r dt = \frac{-2nv_{r0}f_s}{\pi Z_r f_r}. \tag{13}$$

v_{r0} can be calculated based on the output current I_o. In other words, the resonant current and voltage are up to the output current. Large output current could lead to high resonant current and voltage.

C. Boundary Conditions

In the proposed control-free battery charger, the CC and CV operation modes are decided by the load conditions. To ensure the converter works in the CC mode, the following three conditions should be satisfied.

$$V_i - v_{\mathrm{r0}} \geq nV_{\mathrm{bat}}, \tag{14}$$

$$v_{\mathrm{r1}} \geq nV_{\mathrm{bat}}, \text{ and,} \tag{15}$$

$$|v_{\mathrm{r2}}| \leq V_i. \tag{16}$$

To be specific, (14) makes D_1 and D_4 ON during Stage 1, (15) ensures D_2 and D_3 are ON during Stage 2 to make the rectifier conduct during 0 ~ T_r, and (16) ensures that the primary switch anti-parallel diodes can block the input voltage and make the resonant current discontinuous during T_r ~ $T_s/2$.

Using (7) to (16), the boundary condition between CC and CV mode can be achieved.

$$V_i = nV_{\mathrm{bat}}. \tag{17}$$

With the increase of load resistor, nV_{bat} could rise. Once V_{bat} reaches V_i/n, the rectifier could disconnect at stage 2, then CC charging will not be maintained, the converter automatically enters into the CV mode. According to (10) and (17), the critical load resistor $R_{\mathrm{L,\ cri}}$ between CC and CV modes are

$$R_{\mathrm{L,\ cri}} = \frac{\pi Z_r f_r}{2n^2 f_s}. \tag{18}$$

In the CC-CV charging method, firstly the battery voltage is low and a large current is needed to accelerate the charging speed. The load resistor could be very small and the converter works in the CC mode. The current is constant while the voltage rise from 0 to nV_{bat}, i.e. the equal resistor rise from 0 to $R_{\mathrm{L,\ cir}}$. Specifically, the charging current is proportional to the switching frequency, making it can be flexibly set by choosing a suitable frequency. Therefore, both slow charging with $0.1C$ and fast charging with $2C$ can be realized by the proposed method.

Battery voltage could rise with the increasement of battery state of charge (SOC) as well as the load resistor. When the load resistor is larger than $R_{\mathrm{L,\ cri}}$, the proposed converter could automatically transfer to the CV mode. The voltage is constant while the current falls to 0, i.e. the equal resistor rise from $R_{\mathrm{L,\ cir}}$ to infinite. The battery voltage is clamped to V_i/n given in (12) and the charging current falls as the load resistor rises. The battery maximum safe threshold value can be obtained by regulating the input voltage V_i.

With the increase of the load, the proposed converter can automatically enter CV mode without state-of-charge detection and active control. In other words, the proposed control-free battery charger enables automatic CC-to-CV transition. During the operation, the switching frequency is fixed rather than variable. Given a switching frequency, the automatic CC-to-CV feature can be achieved without any active control. Nevertheless, the switching frequency can be configured to achieve different CC outputs.

III. Design Consideration

To implement the CC-CV features, the resonant tank of the converter should be carefully designed according to the battery charging requirements, the maximum charging current $I_{o,\max}$ in the CC mode, and the safe threshold voltage value $V_{\mathrm{bat,\ max}}$ in the CV mode.

A. Resonant Tank

The design procedure of the resonant tank is given as follows.

1) Step 1: choose the maximum charging current $I_{\mathrm{o,\ max}}$ and input voltage V_i. Choose the maximum switching frequency $f_{\mathrm{s,\ max}}$.
2) Step 2: determine the resonant frequency f_r, which is

$$f_r \geq 2f_{\mathrm{s,\ max}}. \tag{19}$$

3) Step 3: calculate the characteristic impedance Z_r, which should satisfy

$$Z_r \leq \frac{2nV_i f_{\mathrm{s,max}}}{\pi f_r I_{\mathrm{o,\ max}}}. \tag{20}$$

4) Step 4: design the resonant tank.

$$L_r = \frac{Z_r}{2\pi f_r}, \text{ and} \tag{21}$$

$$C_r = \frac{1}{2\pi f_r Z_r}. \tag{22}$$

B. Transformer

As shown in Fig. 1, the transformer voltage is equal to v_{cd} that decides the magnetic flux density B and magnetic current.

1) CC Mode: Transformer voltage v_{cd} decides the varying ratio of magnetic current i_m. When v_{cd} is clamped to V_{bat}, i_m could linearly rise for half resonant cycle. Then v_{cd} reverses to $-V_{\mathrm{bat}}$ leading to linearly decrement of i_m. Finally, v_{cd} is shortened by the damping circuit making i_m keep zero. According to the i_m waveform, B_m is given as

$$B_m = \frac{V_{\mathrm{bat,\ max}}}{2f_r N_2 A_e}, \tag{23}$$

2) CV Mode: Similarly, i_m also linearly rises for the first half cycle due to $v_{cd} = V_{\mathrm{bat}}$. During the next half resonant cycle, v_{cd} is clamped to $-v_{r1}/n$, the maximum value of which is V_{bat}. In stage 3, i_m could quickly fall to zero due to the damping resistor and keep zero until to half switching cycle. Therefore, B_m is the same as the one in the CC mode which is given in (23).

Considering the worst conditions, the practical magnetic flux density B should be smaller than the maximum value. Thus the minimum turns ratio is derived as

$$N_2 = \frac{V_i}{2 f_r B_m n A_e}, \tag{24}$$

where n is the transformer turn ratio decided by

$$n = \frac{V_i}{V_{\text{bat, max}}}. \tag{25}$$

It should be noticed that because the transformer is shortened during the variable period T_r ~ $T_s/2$, the transform design is decided by the resonant frequency not the minimum switching frequency. Thus the transformer size and core loss are not large even for a small switching frequency.

IV. Loss Analysis

The power loss of the converter mainly consists of switcher loss and magnetic devices loss (inductor and transformer). The switcher loss can be divided into switching loss and conduction loss. And magnetic device losses include conduction loss and core loss. It's necessary to consider all four sources of loss to improve the converter efficiency.

A. Loss of Power Switches

1) Switching loss: According to the analysis in Section II, all switchers realize both ZCS-ON and -OFF. Only the turn OFF loss caused by the parasitic capacitance should be calculated, which is

$$P_{\text{OFF}} = \frac{1}{2} p C_{ds} V_{ds}^2 f_s, \tag{26}$$

Please note that, fully zero current switching (ZCS), not only means ZCS-ON but also ZCS-OFF, while typically only sole ZVS-ON can be realized in conventional methods. Compared with conventional modulation scheme with sole ZVS-ON, fully ZCS ON and OFF help in achieving high efficiency for the following reasons.

1) First, the switching loss can be reduced. Commonly, conventional modulation only achieves ZVS-ON, but suffers from hard switching OFF. The total switching loss is given by $\frac{1}{2} V_{\text{ds}} i_{\text{off}} t_{\text{off}} f_s$, where i_{off} is the instantaneous current value when switch turns OFF and t_{off} is the turning-OFF time. When i_{off} is large due to phase lag or heavy load, the hard switching OFF loss is significant. Whereas, the proposed modulation, realize both ZCS ON and OFF simultaneously, the total switching loss is only $\frac{1}{2} C_{\text{ds}} V_{\text{ds}}^2 f_s$. The ZCS-ON loss is small due to small junction capacitance C_{ds} (usually pF level) and regardless of load conditions.
2) Second, the conduction loss can be reduced. Since the proposed modulation realizes fully ZCS ON and OFF (similar to sinusoidal modulation), the backflow power can be eliminated. The resonant current is in phase with the terminal voltage, and the conduction loss is reduced. However, the conventional modulations that cannot eliminate backflow power will incur higher conduction loss. That is a major reason why the proposed modulation enables high efficiency throughout the whole load range, while the conventional modulations suffer from efficiency deviation in the light load conditions.
3) Third, fully ZCS ON and OFF can be achieved over the whole load range. Commonly, the conventional modulations meet difficulties in maintaining ZVS-ON over a wide output range, especially in light load condition. In the proposed method, the fully ZCS-ON and -OFF are regardless of the load conditions.

For the reasons above, fully ZCS ON and OFF is an important characteristic of the proposed modulation, and it helps in high efficiency throughout the whole load range.

2) Conduction Loss: The conduction loss of the switchers is up to the RMS value of resonant converter $I_{r,\ \text{RMS}}$, which is decided by

$$P_{sw.,\ cond.} = \frac{1}{2} I_{r,\ \text{RMS}}^2 r_{sw.}, \tag{27}$$

According to (1) and (4), $I_{r,\text{RMS}}$ in CC mode is given as

$$I_{r,\text{RMS}} = \frac{1}{Z_r} \sqrt{\frac{f_s}{2 f_r} [(n V_{\text{bat}})^2 + (V_i - n V_{\text{bat}})^2]}. \tag{28}$$

The conduction loss in the CC mode is in proportion to f_s, similar to the output power. Thus f_s has no effect on the efficiency.

Similarly, in the CV mode, $I_{r,\text{RMS}}$ can be calculated as

$$I_{r,\text{RMS}} = \frac{I_o \pi}{2n} \sqrt{\frac{f_r}{2 f_s}}. \tag{29}$$

Large f_s leads to small conduction loss in the CV mode, providing higher efficiency.

B. Losses of Magnetic Devices

The transformer and resonant inductor are the two magnetic devices in the converter, which have similar power loss. This subsection only analyzes the power loss of transformer.

1) Transformer Conduction Loss: The conduction loss of the transformer is also decided by $I_{r,\ \text{RMS}}$, which has been illustrated above. The conduction loss can be calculated by

$$P_{tr.,\ cond.} = I_{r,\ \text{RMS}}^2 r_{tr.}, \tag{30}$$

2) Transformer Core Loss: Commonly, the generalized Steinmetz equation (GSE) can be used to accurately calculate the transformer core loss, which is given as

$$P_{tr.,\ core} = V_T \frac{1}{T_s} \int_0^{T_s} k_1 \left|\frac{dB}{dt}\right|^{\alpha} |B(t)|^{\beta-\alpha} dt. \tag{31}$$

The coefficient k_1 is given by

$$k_1 = \frac{k}{(2\pi)^{\alpha-1} \int_0^{2\pi} |\cos\theta|^{\alpha} |\sin\theta|^{\beta-\alpha} d\theta}, \tag{32}$$

The transformer core loss only occurs when magnetic flux density B varies.

As the illustration in Section II, during $T_r/2$ ~ $T_s/2$, switchers S_{s1} and S_{s2} are ON shortening the transformer.

TABLE I
SPECIFICATIONS AND PARAMETERS OF THE SRC

Specifications		Symbols	Values
Primary side	Voltage range	V_i	400 V
	Current range	i_{in}	0 – 2.5 A
Secondary side	Voltage range	V_{bat}	0 – 420 V
	Current range	i_o	0 – 2.5 A

Parameters	Symbols	Values
Primary-side switches	S_1 – S_4	C3M0065090D
Secondary-side diodes	D_1 – D_4	NXPLQSC30650W6Q
Damping-circuit switches	S_{s1} – S_{s2}	C3M0065090D
Resonant inductor	L_r	20 μH
Magnetic inductance	L_m	3.02 mH
Resonant capacitor	C_r	32 nF
Damping resistor	R_d	50 Ω
Resonant frequency	f_r	200 kHz
Turn ratio	n	18:19
Switching frequency	f_s	0 – 100 kHz

The transformer's B could be constant providing no core loss during this period. The core loss of the converter can be rewritten as

$$P_{tr.,\ core} = V_T k(\frac{f_r}{2})^{\alpha-1} B_m^{\beta} f_s. \tag{33}$$

B_m is calculated by (23), which is decided by the high resonant frequency f_r. Compared to the traditional methods where core loss is up to the minimum switching frequency, a smaller core loss can be obtained by the proposed modulation. Moreover, the transformer core loss is linearly proportional to f_s, similar to the output power in the CC mode. f_s has no effect on the efficiency.

In conclusion, high efficiency was achieved for the following reasons.

1) First, he switching loss is tiny. Both ZCS-ON and -OFF simultaneously are realized over a wide output range in the proposed method, the total switching loss is regardless of the load conditions, which is only $1W$ in this paper.
2) Second, the conduction loss is small. A zero phase angle between the input voltage and current is obtained during the whole charging process in the proposed method. Whereas, large backflow current is needed in the conventional method which results into large conduction loss.
3) Third, the magnetic core loss is small. Commonly, large switching frequency could lead to large magnetic core loss. In conventional method, the switching frequency varies with the load and is larger than the resonant frequency. Whereas, the switching frequency is fixed in the paper and is only a quarter of the resonant frequency. Thus the magnetic core loss is significantly reduced.

High efficiency can be achieved during the whole CC-CV charging process.

V. EXPERIMENTAL VERIFICATION

A 1 kVA experimental prototype of SRC is built with specifications and parameters given in Table I. The experimental setup is shown in Fig. 4. A electronic load is used to emulate the practical battery. Both Constant Resistance (CR)

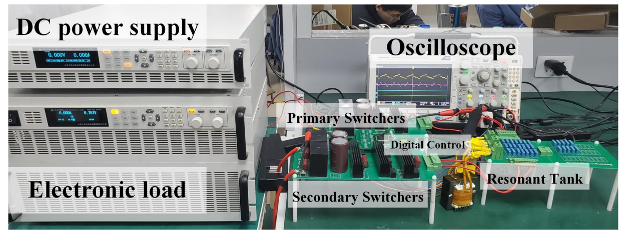

Fig. 4. Experiment setup.

and Constant Voltage (CV) modes are used depending on the testing purposes. In the experiment, the SRC works in the CC mode (i_o=2.5 A) and the CV mode (V_{bat} = 420 V).

A. Operating Waveforms

The operating and soft switching waveforms are captured in Fig.5 and Fig. 6 depicting the CC and CV modes respectively.

In the CC mode, the input voltage is $V_i = 400$ V, the output current is $i_o = 2.5$ A. The electronic load works in CR mode, and the resistance is $R_{\text{L}} = 40\Omega$. The output voltage is $V_{\text{bat}} =$ 100 V and $f_s = 52$ kHz. v_{ab}, v_{cd} and i_r are consistent with the operating principle for the CC operating mode analyzed in Section II-B as show in Fig.5(a).

In Stage 1, v_{ab} and v_{cd} are both high level; in Stage 2, v_{ab} is zero level and v_{cd} is negative level; in Stage 3, v_{ab} is resonating with C_p and R_d and quickly damped to zero, while v_{cd} is zero level. The waveform of i_r is sinusoidal and in phase with v_{ab} as well as v_{cd}, therefore, there is no backflow power.

The soft switching waveforms of S_1 and S_3 are given in Fig.5(b) and Fig.5(c), while the switching waveforms of S_2 and S_4 are similar to S_1 and S_3 which are not repeated here. The switches turn ON and OFF when the current is close to zero realizing ZCS-ON and ZCS-OFF simultaneously.

In the CV mode, $V_i = 400$ V, $V_{\text{bat}} = 420$ V. The electronic load works in CR mode and the resistance is $R_{\text{L}} = 266\Omega$. Then $i_o = 1.58$ A and $f_s = 52$ kHz. v_{ab}, v_{cd} and i_r are consistent with the operating principle for the CV operating mode analyzed in Section II-C as show in Fig.6(a).

When v_{ab} and v_{cd} are both high levels for half the resonant period, then v_{ab} changes to zero for the next half resonant period, while v_{cd} is resonating with magnetic inductance and is negative level. For the rest time of the half switching period, the waveforms of v_{ab} and v_{cd} are similar to the CC mode. The waveform of i_r slightly falls which can be regarded as invariable during the second half of the resonant period, then is zero for the rest time of the half switching period. Therefore, there is no backflow as well.

The soft switching waveforms of S_1 and S_3 are given in Fig.6(b) and 6(c), while the switching waveforms of S_2 and S_4 are similar to S_1 and S_3 respectively. All switches turn ON and OFF when the current is close to zero realizing ZCS-ON and ZCS-OFF simultaneously.

Noticeably, in Fig. 6(a), the high ringing effect appears in stage 2, which is caused by the resonance between resonant tank, magnetic inductance and transformer winding capacitance. Fortunately, the high ring can be clamped by the output voltage and primary switches shorten the terminal voltage. The

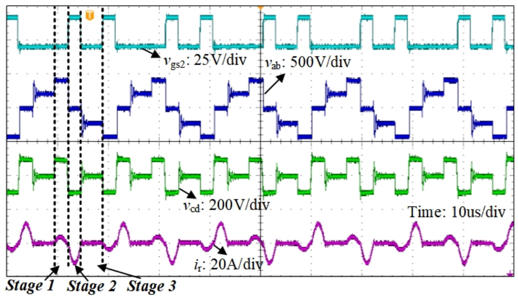

(a) Terminal voltage and resonant current waveforms.

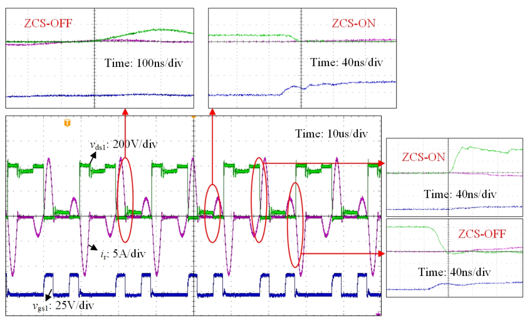

(b) Soft switching waveforms of S_1.

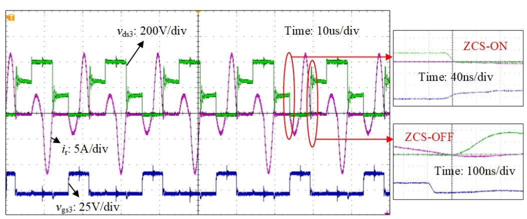

(c) Soft switching waveforms of S_3.

Fig. 5. Operation waveforms of the SRC for CC mode.

high ringing effect has no effect on the switches and input and output sides.

B. Transient Waveforms

Fig 7 shows the transient waveforms from the CC mode to the CV mode. The SRC works without control during the whole transient conditions. The electronic load operates in CV mode with a small resistance about 1Ω in series. The output voltage is changed from 250 V to 418 V. The output current could fail from 2.5 A to 2 A and the equal load resistance rises from 100 Ω to 200 Ω.

Auto transient from CC to CV mode can be obtained, which is perfectly suitable for the battery charging process.

C. Measured Output Characteristics

The measured output current i_o and voltage $V_{\rm bat}$ versus the equal load resistance is shown in Fig. 8. During the CC mode, i_o is maintained to 2.5 A with fixed $f_s = 52$ kHz while $V_{\rm bat}$ rises with the increase of the load resistance R_L. When R_L is about 168 Ω, the converter enters into CV mode. $V_{\rm bat}$ is nearly invariable and slightly rises to 420 V with the decrease of i_o. Wide operating range and automatic CC-CV transition are achieved, obtaining control-free features.

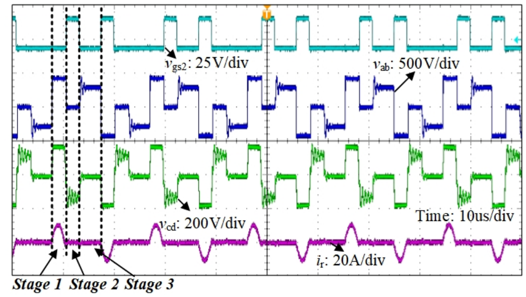

(a) Terminal voltage and resonant current waveforms.

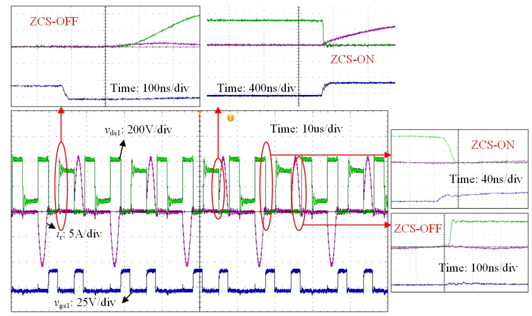

(b) Soft switching waveforms of S_1.

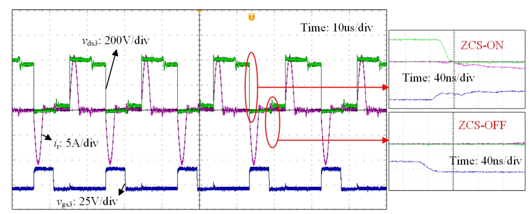

(c) Soft switching waveforms of S_3.

Fig. 6. Operation waveforms of the SRC for CV mode.

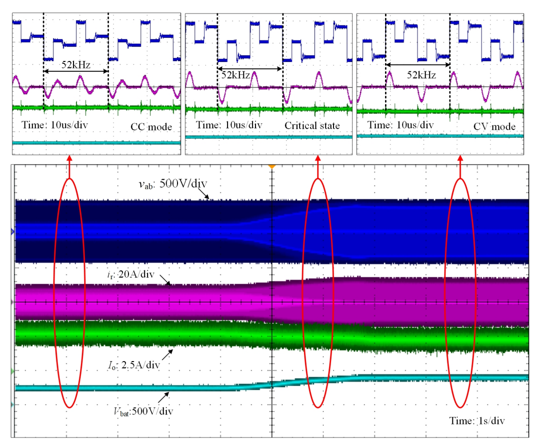

Fig. 7. Transition waveforms from CC to CV mode.

D. Measured Efficiency

Measured efficiency and power versus load resistance are given in Fig. 9, where i_o is fixed to 2.5 A in the CC mode, and $V_{\rm bat}$ is fixed to 420 V in the CV mode. The delivered power rises with the increase of $V_{\rm bat}$ in the CC mode and falls as i_o decreases during the CV mode, achieving the peak power 1000 W at the point of CC-CV.

It can be observed that the peak efficiency of the converter is

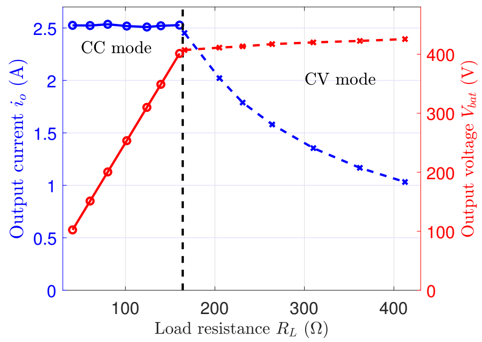

Fig. 8. Measured i_o and $V_{\rm bat}$ versus load resistance.

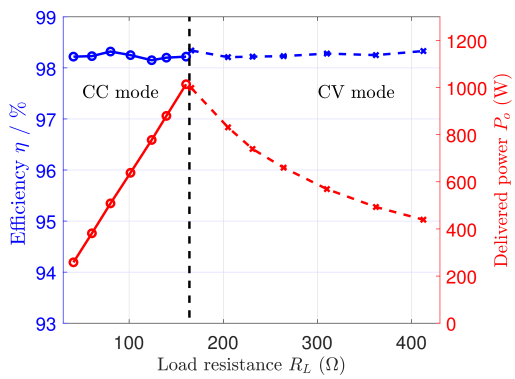

Fig. 9. Measured efficiency and power versus load resistance.

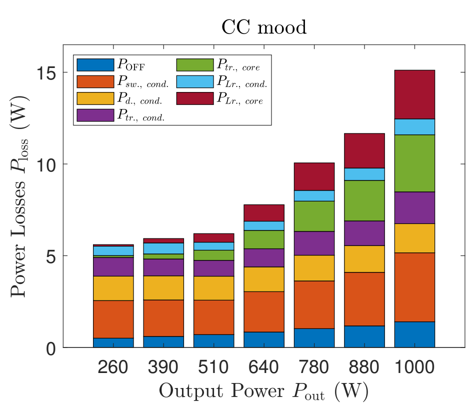

(a) Loss breakdown for V_i=400V and i_o=2.5A.

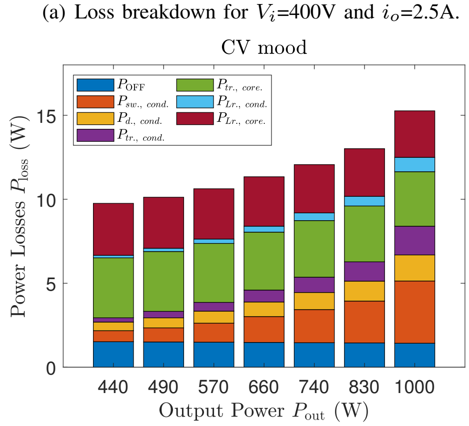

(b) Loss breakdown for V_i=400V and $V_{\rm bat}$=420V.

Fig. 10. Power loss breakdown for CC and CV modes.

near 98.4%, and the efficiency ranges from 98.1% and 98.4% during the whole CC and CV process. Fig. 10 also depicts the power loss breakdown. High efficiency can be achieved for the whole operating range, which perfectly adjusts the battery charging applications.

VI. Conclusion

To achieve CC and CV outputs for the battery charging applications, this paper proposes a control-free battery charger based on SRC. Wide voltage range from 0 to rated value and wide load range from 0 to the rated power are acquired. Inherent f_s controlled current independent-voltage and V_i controlled voltage independent-current are obtained realizing accurate and control-free CC and CV outputs. Automatic and smooth CC-CV transition is also achieved by tackling the overcharging risk. Moreover, fully soft switching is realized for all switches during the whole operating range, achieving high efficiency up to 98.4%. Experiment results validate the analysis well.

References

[1] M. Jahnes, L. Zhou, M. Eull, W. Wang and M. Preindl, "Design of a 22kW transformerless EV charger with V2G capabilities and peak 99.5% Efficiency," *IEEE Trans. Ind. Electron.,* Early Access, July. 2022.

[2] M. Yilmaz and P. T. Krein, "Review of battery charger topologies charging power levels and infrastructure for plug-in electric and hybrid vehicles," *IEEE Trans. Power Electron.,* vol. 28, no. 5, pp. 2151-2169, May 2013.

[3] Z. Fang, Z. Wei, Z. Huang and F. Liu, "Onboard energy storage system based on interleaved high-conversion-ratio quasi-resonant converter with small characteristic impedance," *IEEE Trans.Vehi. Tech.,* vol. 70, no. 5, pp. 4238-4251, May. 2021.

[4] F. Liu, X. Ruan and Y. Jiang, "DCX-LLC resonant converter based two-stage DC-DC converter," *IEEE Trans. Ind. Electron.,* Early Access, July. 2022.

[5] F. Musavi, M. Craciun, D. S. Gautam, W. Eberle and W. G. Dunford, "An LLC resonant DC-DC converter for wide output voltage range battery charging applications," *IEEE Trans. Power Electron.,* vol. 28, no. 12, pp. 5437-5445, Dec. 2013.

[6] J. Deng, S. Li, S. Hu, C. C. Mi and R. Ma, "Design methodology of LLC resonant converters for electric vehicle battery chargers," *IEEE Trans. Vehi. Tech.,* vol. 63, no. 4, pp. 1581-1592, May. 2014.

[7] X. Fang, H. Hu, Z. J. Shen and I. Batarseh, "Operation mode analysis and peak gain approximation of the LLC resonant converter," *IEEE Trans. Power Electron.,* vol. 27, no. 4, pp. 1985-1995, Apr. 2012.

[8] Z. Fang, T. Cai, S. Duan and C. Chen, "Optimal design methodology for LLC resonant converter in battery charging applications based on time-weighted average efficiency," *IEEE Trans. Power Electron.,* vol. 30, no. 10, pp. 5469-5483, Oct. 2015.

[9] N. Shafiei, M. Ordonez, M. Craciun, C. Botting, and M. Edington,"Burst mode elimination in high-power LLC resonant battery charger for electric vehicles," *IEEE Trans. Power Electron.,* vol. 31, no. 2, pp. 1173-1188, Feb. 2016.

[10] H. Zeng, N. Gonzalez-Santini, Y. Yu, S. Yang, and F. Peng, "Harmonic burst control strategy for full-bridge series resonant converter-based EV charging," *IEEE Trans. Power Electron.,* vol. 32, no. 5, pp. 4046-4073, May 2017.

[11] B. C. Kim, K. B. Park and G. W. Moon, "Asymmetric PWM control scheme during hold-up time for LLC resonant converter," *IEEE Trans. Ind. Electron.,* vol. 59, no. 7, pp. 2992 - 2997, Jul. 2012.

[12] H. Wu, X. Zhan, and Y. Xing, "Interleaved LLC resonant converter with hybrid rectifier and variable-frequency plus phase-shift control for wide output voltage range applications," *IEEE Trans. Power Electron.,* vol. 32, no. 5, pp. 4246-4257, May 2017.

[13] Z. Fang, J. Wang, R. Liu. et. al.,"Energy feedback control of light-load voltage regulation for LLC resonant converter," *IEEE Trans. Power Electron.,* vol. 34, no. 5, pp. 4807 - 4819, May. 2019.

[14] K. W. Kim, H. S. Youn, J. I. Baek, Y. Jeong, and G. W. Moon, “Analysis on synchronous rectifier control to improve regulation capability of high-frequency LLC resonant converter,” *IEEE Trans. Power Electron.,* vol. 33, no. 8, pp. 7252-7259, Aug. 2018.
[15] Y. Gu, Z. Lue, L. Huang, Z. Qian, and G. Huang, “Three-level LLC series resonant DC/DC converter,” *IEEE Trans. Power Electron.,* vol. 20, no. 4, pp. 781-789, Jul. 2005.
[16] S. Zhao, A. Kempitiya, W. T. Chou, V. Palija and C. Bonfiglio, “Variable DC-link voltage LLC resonant DC/DC converter with wide bandgap power devices,” *IEEE Trans. Ind. App.,* vol. 58, no. 3, pp. 2965-2977, May-Jun. 2022.
[17] B. Li, Q. Li, Fred C. Lee, Z. Liu, and Y. Yang, “A high-efficiency high-density wide-bandgap device-based bidirectional on-board charger,” *IEEE J. Emerg. Sel. Topics Power Electron.,* vol. 6, no. 3, pp. 1627-1636, Sep. 2018.
[18] F. C. Lee, Q. Li and A. Nabih “High frequency resonant converters: an overview on the magnetic design and control methods,” *IEEE J. Emerg. Sel. Topics Power Electron.,* vol. 9, no. 1, pp. 11-23, Jul. 2020.
[19] S. W. Kang and B. H. Cho, “Digitally implemented charge control for LLC resonant converters,” *IEEE Trans. Power Electron.,* vol. 64, no. 8, pp. 6159-6168, Aug. 2017.
[20] Z. Fang, J. Wang, S. Duan, K. Liu and T. Cai, “Control of an LLC resonant converter using load feedback linearization,” *IEEE Trans. Power Electron.,* vol. 33, no. 1, pp. 887-898, Jan. 2018.
[21] A. Nabih, M. Ahmed, Q. Li and F. C. Lee, “Transient control and soft start-up for 1 MHz LLC converter with wide input voltage range using simplified optimal trajectory control,” *IEEE J. Emerg. Sel. Topics Power Electron.,* vol. 9, no. 1, pp. 24-37, Feb. 2021.
[22] V. B. Vu, D. H. Tran and W. Choi, “Implementation of the constant current and constant voltage charge of inductive power transfer systems with the double-sided LCC compensation topology for electric vehicle battery charging applications,” *IEEE Trans. Power Electron.,* vol. 33, no. 9, pp. 7398-7410, Sep. 2018.
[23] J. Lu, G. Zhu, D. Lin, Y. Zhang, J. Jiang and C. C. Mi, “Unified load-independent ZPA analysis and design in CC and CV modes of higher order resonant circuits for WPT system,” *IEEE Trans. Transp. Electrif.,* vol. 5, no. 4, pp. 977-987, Dec. 2019.
[24] X. Qu, H. Han, S. C. Wong, C. K. Tse and W. Chen, “Hybrid IPT topologies with constant current and constant voltage output for battery charging applications,” *IEEE Trans. Power Electron.,* vol. 30, no. 11, pp. 6329-6337, Nov. 2015.
[25] T. N. Gucin, M. Biberoglu and B. Fincan, “Constant frequency operation of parallel resonant converter for constant-current constant-voltage battery charger applications,” *J. Mod. Power Syst. Clean Energy,* vol. 7, no. 1, pp. 186-199, Jan. 2019.
[26] M. Borage, S. Tiwari and S. Kotaiah, “Analysis and design of LCL-T resonant converter as a constant-current power supply,” *IEEE Trans. Ind. Electron.,* vol. 52, no. 6, pp. 1547-1554, Dec. 2005.
[27] M. Borage, S. Tiwari and S. Kotaiah, “LCL-T resonant converter with clamp diodes: a novel constant-current power supply with inherent constant-voltage limit,” *IEEE Trans. Ind. Electron.,* vol. 54, no. 2, pp. 741-746, Apr. 2007.
[28] H. H. Vu and W. Choi, “A novel dual full-bridge LLC resonant converter for CC and CV charges of batteries for electric vehicles,” *IEEE Trans. Ind. Electron.,* vol. 65, no. 3, pp. 2212-2225, Mar. 2018.

Zhijian Fang (M’13) received the B.S. and Ph. D degree in electrical engineering and automation from Huazhong University of Science and Technology, Wuhan, China in 2010 and 2015, respectively.

From 2015 to 2018, he is a post-doctoral research fellow with the school of electrical engineering, Wuhan University, Wuhan, P. R. China. From Feb. 2016 to Jan. 2017, he was a post-doctoral research fellow with department of electrical and computer engineering, Ryerson University, Toronto, Canada. Since 2019, he is a Professor with the School of Automatic, China University of Geosciences (Wuhan). His research interests include high performance DC/DC converter, battery charger and renewable energy applications

Haojiang Yue received the bachelor’s degree in automation from China University of Geosciences, Wuhan, China, in 2020. He is currently working toward the master’s degree in control engineering with the China University of Geosciences, Wuhan, China. His research focuses on DC/DC resonant converter.

Zihao Wei received the bachelor’s degree in electrical engineering and automation from Harbin Institute of Technology, Harbin, China, in 2018. He is currently working toward the master’s degree with the Department of control science and engineering, China University of Geosciences, Wuhan, China. His research mainly focuses on dc-dc converter and its control method.

Zihan Zhang graduated from Yanshan University with a bachelor’s degree in electrical engineering in 2021. He is studying for a master’s degree in at China University of Geosciences, Wuhan. He studies and works in School of Automation. His field of research includes Power Electronics and Energy Harvesting.

Zhicong Huang (Member, IEEE) received the B.Eng. degree in electrical engineering and automation and the M.Eng. degree in mechanical and electronic engineering from the Huazhong University of Science and Technology, Wuhan, China, in 2010 and 2013, respectively, and the Ph.D. degree in power electronics from The Hong Kong Polytechnic University, Hong Kong, in 2018.

He is currently an Associate Professor with the Shien-Ming Wu School of Intelligent Engineering, South China University of Technology, Guangzhou, China. From January 2019 to February 2020, he was a Postdoctoral Fellow under the UM Macao Talent Program, with the State Key Laboratory of Analog and Mixed-Signal VLSI, University of Macau, Macao, China. His research interests include wireless power transfer, power electronics penetrated power system, electric vehicle, and intelligent engineering.

Dr. Huang received the Outstanding Reviewer Award from IEEE TRANSACTION ON POWER ELECTRONICS in 2021.